

DYNAMIC FRACTURE OF CONCRETE IN COMPRESSION: 3D FINITE ELEMENT ANALYSIS AT MESO- AND MACRO-SCALE

S. GAMBARELLI* AND J. OŽBOLT†

* Materials testing Institute, University of Stuttgart
Pfaffenwaldring 4c, 70569 Stuttgart, Germany
e-mail: serena.gambarelli@mpa.uni-stuttgart.de

† Institute of Construction Materials, University of Stuttgart
Pfaffenwaldring 4, 70569 Stuttgart, Germany
e-mail: ozbolt@iwb.uni-stuttgart.de

Key words: impact loads, rate sensitivity, dynamic fracture, mesoscale modeling, microplane material model

Abstract: In the present paper fracture of normal strength concrete under static and dynamic compressive loading is numerically investigated. 3D finite element simulations are carried out at macro- and meso-scale. At meso-scale the analysis is performed with and without accounting for the interface zone (IZ) between aggregate and mortar. Aggregate is assumed to be linear elastic and mortar is modeled using rate-dependent microplane model. In the framework of the study the differences between meso- and macro-modeling approaches are investigated. It is shown that the macroscopic analysis is principally able to account for the major effects related to the dynamic fracture of concrete and that the IZ has not strong influence on the response of concrete. Dynamic resistance of concrete in compression (apparent strength) depends on a number of parameters and it is mainly influenced by the structural inertia effects that are closely related to the load induced damage.

1 INTRODUCTION

Understanding dynamic fracture behavior of concrete at high strain rates is fundamental for the safety assessment and design of concrete structures subjected to dynamic loading (impact and blast). It is well known that the behavior of concrete structures is strongly influenced by the loading rate [1]. Compared to quasi-static load, concrete under impact load acts in a different way. First, there is a strain-rate influence on strength, stiffness, and ductility, and, second, there is inertia activated which influence the resistance and failure mode of concrete. The results of dynamic experimental tests show that after reaching some critical strain rate concrete

resistance progressively increases with increase of strain rate. This type of response is typical for many different problems, e.g. compression, direct tension, bending, pull-out of anchors, etc. [1,2].

The compressive strength of concrete under dynamic loading is usually tested using hydraulic machines, drop hammers machines and split Hopkinson pressure bars (SHPB). The first two allow testing all shapes and sizes of the specimens with Length/Diameter (L/D) ≥ 2 [3]. However, they are not able to achieve strain rates higher than 10 s^{-1} . The SHPB can attain strain rates between $10^0 \div 10^4 \text{ s}^{-1}$, but the variety of dimensions of the specimens is very small (with $L/D = 0.3 \div 1$) to

ensure the proper functioning of the setup. Independently of the used testing technique, all the available experimental data show that the dynamic compressive resistance of concrete increases with the increase of the strain rate [4-13]. Based on the available tests results, the compressive dynamic increase factor (CDIF), defined as the ratio of dynamic to static resistance, has been introduced to derive some empirical formulae evaluating the strength enhancement as a result of the strain rate effect [8-11,14-16].

Although the definition of dynamic compressive strength through the CDIF factor has attracted considerable interest in structural design, it should be pointed out that the strength enhancement of concrete at high loading rates is not a material property. As shown in [17], a relevant scatter of the CDIF data has been detected in all available experimental tests. The reasons for the contrasting results have been widely discussed, with the conclusion that the strength enhancement of concrete under dynamic compressive loading is influenced by several parameters, partially related to the material itself and partially to the structural effects. For relatively low loading rates the moderate increase of resistance with increasing loading rate is mainly controlled by the strain rate-dependent response of concrete. This is partly due to the inertia at material micro-scale and partly is a consequence of the viscose response of concrete due to the water content. These two effects can be accounted for by the constitutive law. However, the main reason for the progressive increase of resistance with increase of loading rate is activation of inertia at the macro-scale that is due to different reasons such as: structural inertia, inertia due to hardening or softening of concrete, crack propagation and crack branching [1,2,18]. When modeling at meso- or macro-scale these effects should be automatically accounted for [1] whereas the rate effect coming from the material micro level should be covered by the constitutive law. It is important to note that principally the rate sensitive constitutive law should not directly be compared with the results of dynamic test. Namely, to filter out

different effects of inertia the test results must be compared with the results of simulations, i.e. the objective rate sensitive constitutive law can be obtained only by fitting the test results with the results of numerical simulation.

The 3D meso-scale modeling of concrete under dynamic compressive loading is rarely reported in the literature [19]. Thus, in the present paper, the dynamic compressive behavior of normal strength concrete, with strain rate up to 200 s^{-1} , is numerically investigated through 3D macro and meso-scale analysis of a concrete cylinder ($L/D = 2$). To investigate the influence of IZ on the concrete response, e.g. failure mode and contribution to CDIF, the meso-scale simulations are performed with and without IZ. The aim of the study is to clarify whether a meso-scale modeling approach can provide more insights into the dynamic compressive behavior of concrete through explicit modeling of multiple phases (mortar matrix, aggregate and IZ). The paper is organized as follows. Section 2 describes the procedure to generate the meso-scale model, the computational background and the material parameters. In section 3 the obtained results, in terms of stress-strain curves (both load and reaction) and crack patterns, are presented for static and dynamic loading at different strain rates. The results from the meso-analysis (without IZ) are compared with those achieved by using macro-scale model. The influence of IZ (meso-scale analysis) is investigated in section 4. Finally, in section 5 are given the main conclusions.

2 GENERATION OF MESO-SCALE FE MODEL

2.1 Random aggregate structure in concrete

To generate the meso-scale structure of concrete, the coarse aggregate with a specific size distribution, is randomly distributed inside the concrete cylinder, by using a simple generation procedure implemented in Matlab R2013b. The procedure is based on two distance criteria: the first one prevents any contact between the generated particles and the

external boundaries of the cylinder and the second one avoids the intersection between adjacent particles (assumed spherical). As mentioned in the introduction, the meso-scale model is generated with and without interface zone (IZ) between aggregate and mortar. To guarantee the same aggregate distribution in both, bi- and three-phase meso-scale models, the thickness of IZ is accounted for in the above mentioned criteria.

The size distribution of the coarse aggregate is determined by using the Fuller curve (Eq. 1):

$$p(d) = 100 \left(\frac{d}{d_{max}} \right)^q \quad (1)$$

where d is the diameter of each granulometric class, $p(d)$ is the corresponding passing amount (%), d_{max} is the maximum aggregate diameter and q is the exponent of the chosen granulometric curve. The number of particles of each granulometric class is determined as follows: (1) based on the given values of d_{max} and q , the passing amount $p(d)$ is evaluated using Eq. 1; (2) The retained amount (%) is then calculated as the difference between the adjacent classes' passing; (3) Knowing the retained percent of every class, the total volume of the class and the corresponding number of aggregates are evaluated and (4) Spherical particles are randomly placed in the domain, guaranteeing no intersection between any of them.

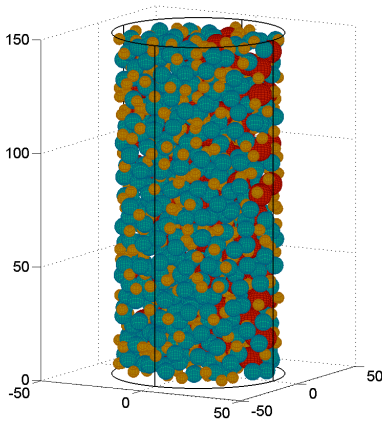


Figure 1: Insertion of particles in the cylinder (three different granulometric sizes)

Based on three different granulometric classes ($d = 5, 7.5, 10$ mm), spheres are inserted from largest to smallest (Fig. 1).

The generated meso-scale models are shown in Fig. 2, where the volume fraction of 28% of the coarse aggregate ($5 \text{ mm} \leq d \leq 10 \text{ mm}$) is reproduced. The geometry of the created meso-models was finally imported into the 3D FE code MASA [20] used for the simulations and meshed with approximately 10^6 solid four-node constant strain finite elements. The same as for the mortar, macro-scale finite element discretization was performed using constant strain four-node finite elements.

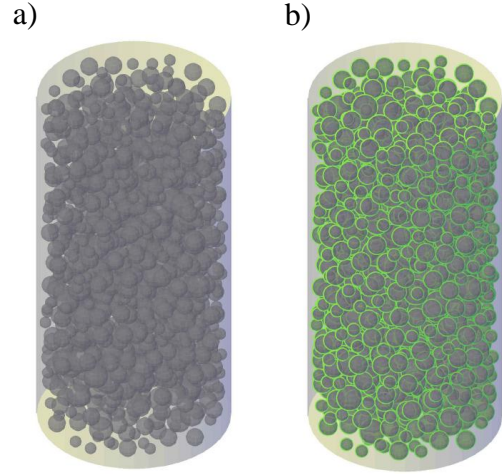


Figure 2: Concrete meso-structure: a) bi-phase material; b) three-phase material

2.2 Material properties

In the meso-scale 3D FE analysis the constitutive laws for mortar and IZ are based on the rate-dependent microplane model proposed by Ožbolt et al. [21], while the aggregate is considered as linear elastic with Young's modulus of 60 GPa and Poisson's number 0.18 (limestone). The ratio of the elastic moduli of the aggregate and matrix phases is set at 3:1, with $E = 20$ GPa. The strength and fracture energy of the IZ are chosen to be approximately 50% of that of mortar. As shown in [22] the Young's modulus of IZ is comparable to that of mortar. The material properties used for the macro and the meso-scale analysis are summarized in Table 1. It is worth mentioning that in both

modeling approaches the model parameters have been calibrated to correctly reproduce the uniaxial compressive behavior of normal strength concrete (see section 3).

Table 1: Material properties (macro- vs. meso-model)

Mechanical properties	Macro-model Concrete	Meso-model		
		Aggr.	Mortar	IZ
E [GPa]	37.0	60.0	20.0	20.0
ν	0.18	0.18	0.18	0.18
f_c [MPa]	23.0	/	26.0	13.0
f_t [MPa]	2.3	/	2.6	1.3
G_F [J/m ²]	60	/	20	10
ρ [T/m ³]	2.3	2.7	2.1	2.1

2.3 Rate-dependent microplane model and 3D FE analysis

In the numerical simulations as a constitutive law the rate sensitive microplane model [21] is employed. In the model the influence of strain rate is accounted for through two effects: (1) the rate dependency due to viscosity of the bulk material and (2) the rate dependent growth of micro-cracks. The influence of structural inertia effects on the rate dependency is not a part of the constitutive law, however, it is automatically accounted for in the dynamic analysis. In the microplane model macroscopic response is obtained by integrating normal and shear microplane stresses overall microplanes. The rate independent microplane stress components $\sigma_{Mp}^0(\varepsilon_{Mp})$ (Mp stands for microplane volumetric, deviatoric and shear components, respectively) are calculated from the known microplane strains ε_{Mp} using pre-defined microplane uniaxial stress-strain constitutive relations [23]. The strain rate independent model parameters are: Young's modulus, Poisson's ratio, uniaxial compressive and tensile strengths and fracture energy. The rate effect on each microplane component is of the same type as proposed by Bažant et al. [24,25].

Static analysis is performed based on the implicit solution scheme whereas in transient 3D dynamic FE analysis the direct integration scheme of explicit type is performed. To get

mesh objective results regularization scheme based on the crack band approach is used [26].

3 INFLUENCE OF STRAIN RATE ON THE CONCRETE COMPRESSIVE FAILURE: MACRO- VS. MESO- ANALYSIS

The influence of the strain rate on dynamic compressive behavior of concrete is investigated by means of macro and meso-scale modeling approaches. 3D FE analysis of concrete cylinder ($L/D = 150/75$ mm) at different strain rates ($50 - 200 \text{ s}^{-1}$) was carried out.

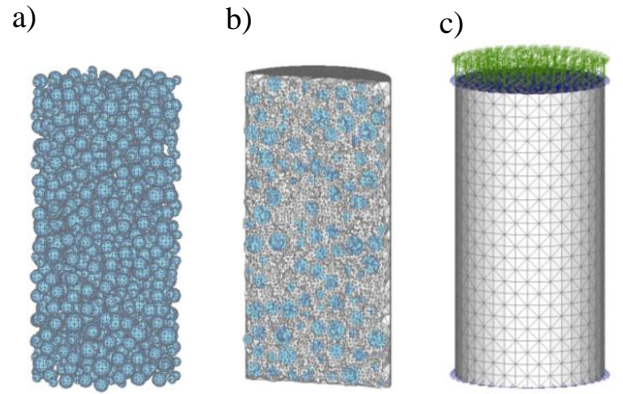


Figure 3: 3D FE meso-scale model: a) coarse aggregate; b) bi-phase material (internal section) and c) FE model with vertical displacement and boundary conditions

Static analysis (no rate effect) was also performed. Upper and lower loading surfaces of the cylinder were fully restrained in the horizontal direction. The load was applied by controlling displacement δ of the upper surface of the cylinder in the vertical direction (Fig. 2). Note that here for the meso-scale analysis bi-phase material model was employed.

3.1 Static analysis

The numerical results, in terms of axial stress-strain curves and concrete failure mode, obtained from the static analysis are shown in Figs. 3 and 4, respectively. It can be seen that both the macro and meso-models are able to correctly reproduce the typical compressive curve of normal strength concrete ($f_c = 23.5$

MPa, $\varepsilon_{peak} = 0.0025$, $E = 27$ GPa) for pre and post-peak responses (Fig. 4).

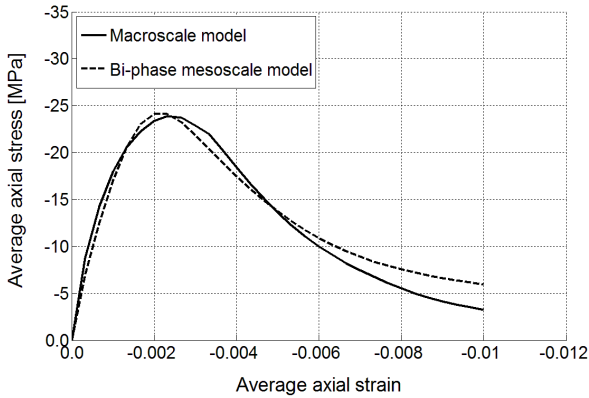
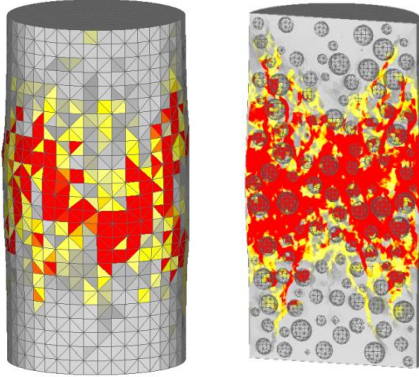


Figure 4: Static uniaxial compressive test: average stress-strain curve

a) Meso-scale analysis



b) Macro-scale analysis

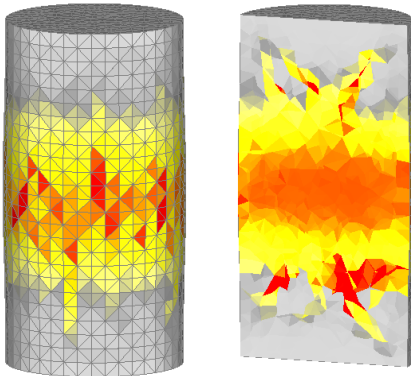


Figure 5: Typical failure mode obtained in the static FE analysis: a) mesoscale and b) macroscale

Note that the internal microplane model parameters were chosen such that static meso- and macro-scale 3D FE analyses give approximately the same response. The typical

failure mode obtained in the static analysis is shown in Fig. 5. Damage in a) mortar and b) concrete is represented in terms of maximum principal strains, where the red zones correspond to the crack width of 0.15 mm or greater. Due to the fixed boundary conditions, diagonal shear failure takes place at the mid of the cylinder height. To show the internal damage distribution the specimen has been cut at mid-section. Similarly as in the experiments, it is possible to recognize the typical hourglass shape of concrete at a final stage of the loading history.

3.2 Dynamic analysis

As mentioned before, the direct integration scheme of explicit type was employed in the dynamic analysis, with damping set to 1000 [N s/mm]. The relatively high value appeared to be necessary because of numerical reasons, i.e. to get the explicit algorithm stable and to prevent local oscillations. The analysis was performed at high strain rate ($50 \div 200$ s⁻¹). The summary of the calculated compressive resistances (loads and reactions) is reported in Table 3. Due to the high loading rates the compressive resistances at loaded top of the cylinder (apparent strength) from the dynamic analysis are significantly higher than the static strength of concrete. However, it can be also seen that the resistance on the reaction (bottom) side of the specimen is only slightly higher than the static strength of the specimen and, as will be shown below, it approximately follows the rate-dependent constitutive law. Actually, the loading stress is much higher than the reaction stress because it must be in equilibrium with structural inertia that is generated as a consequence of concrete damage. This is the same effect as discussed in [2] for the case of uniaxial tension.

From Table 2 can also be seen that the resistance at the loaded side of the cylinder is consistently higher in case of macro-scale model than for the meso-scale model. The reason is due to the fact that the aggregate is linear elastic, i.e. no inertia and rate sensitivity due to damage is generated. Actually, these differences in the apparent strength between

two approaches can be attributed to the effect of inertia induced through the inhomogeneity of concrete, which is in the meso-scale model automatically accounted and in the macro-scale model should be explicitly covered by the rate dependent constitutive law. Consequently, one should here modify the rate dependent model for microplane at macro-scale (parameters c_1 and c_2 in Eq. 2) such that the macro model gives the same result as the meso-scale model. Note that this was not done in the following computations using macro-scale model since the aim here was only to demonstrate that the macro-scale approach is able to principally correctly account for the phenomena related to dynamic fracture of concrete in compression.

Table 2: dynamic analysis – summary of the calculated apparent strength [MPa]

FE Analysis		no rate	50 [s ⁻¹]	100 [s ⁻¹]	150 [s ⁻¹]	200 [s ⁻¹]
Macro scale	Load	23.3	66.8	120.9	170.4	218.5
	Reac.	23.3	45.2	39.4	42.2	67.6
Meso scale	Load	23.8	56.2	100.3	137.1	173.1
	Reac.	23.8	46.8	54.9	58.1	60.0

The typical stress-strain curves for the analyzed strain rates are plotted in Fig. 6. In each graph, both loading and reaction stresses are plotted against the average axial strain. The results from the macro analysis (black curves) are compared with those obtained at meso-scale (red curves). In both cases there is a progressive increase of the loading compressive stress with the increase of loading rate. However, as mentioned above, the reaction stresses are increasing only slightly with the loading rate. Moreover, it can be seen (Fig. 6) that the reaction stress is even not activated at the time when the loading stress reaches its maximum. When increasing the loading rate, the observed delay in the activation of the reaction stress, expressed in terms of average strains, also increases. Note that in terms of time the activation of reaction stress is approximately the same in all cases and it is in the range of 3.2×10^{-5} s.

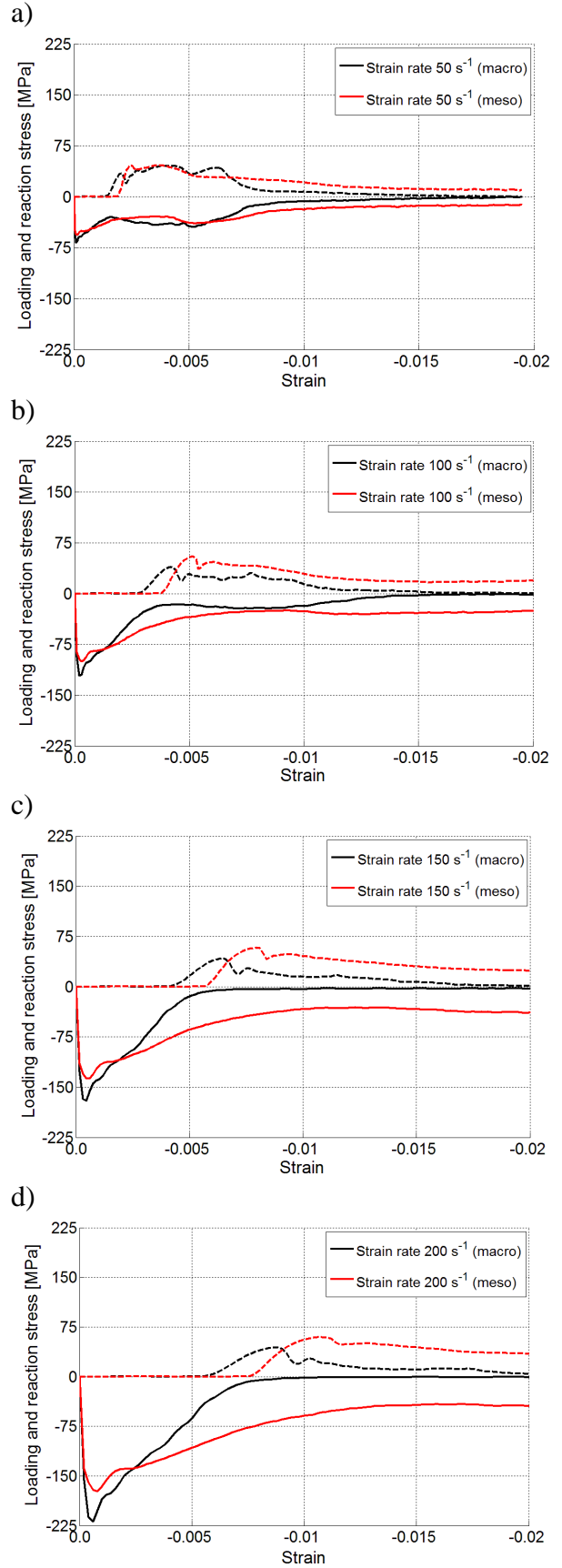


Figure 6: Calculated average stress-average strain curves at different loading rates: a) 50 s^{-1} ; b) 100 s^{-1} ; c) 150 s^{-1} and d) 200 s^{-1}

The evolution of damage in mortar (meso-scale) and concrete (macro-scale), under strain rates 50 and 200 s⁻¹ is shown in Figs. 7, and 8. Concerning the case with strain rate of 50 s⁻¹ (Fig. 7), the damage is mainly localized in the middle part of the specimen and similar results are obtained for both models, i.e. macro and meso. At the end of the loading process, the typical hourglass shape of the specimen as obtained in the static test can be observed (Fig. 7). For very high strain rate (Fig. 8) damage localization takes place in the upper part of the specimen, close to the loading surface. Due to end friction confinement, failure of the specimen occurs slightly away from the loading surface. The results obtained for macro-scale analysis are similar to that achieved at meso-scale, confirming the predictability of both models.

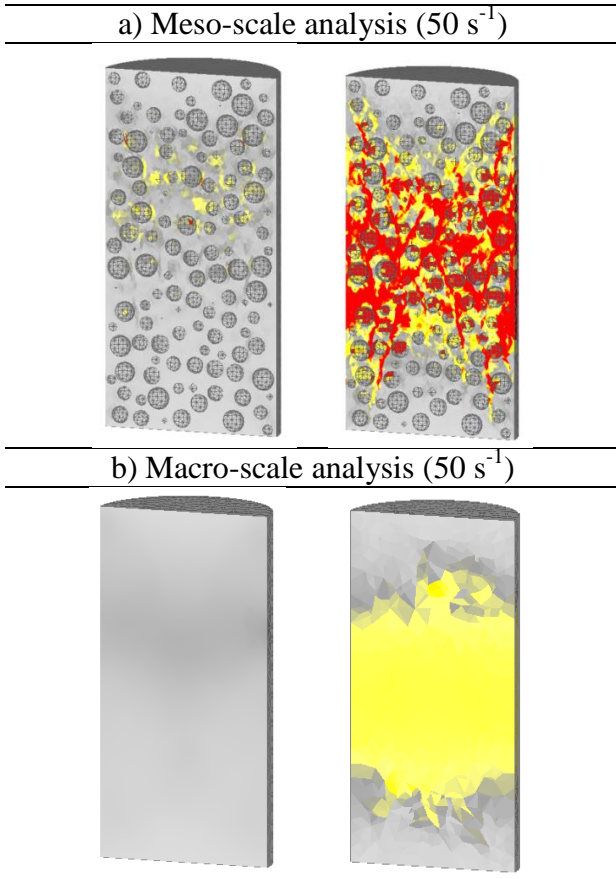


Figure 7: Evolution of damage under strain rate 50 s⁻¹: a) meso-scale analysis; b) macro-scale analysis

As mentioned before, SHPB technique has been widely used to investigate the dynamic

compressive behavior of concrete-like materials at high strain rates [7-10].

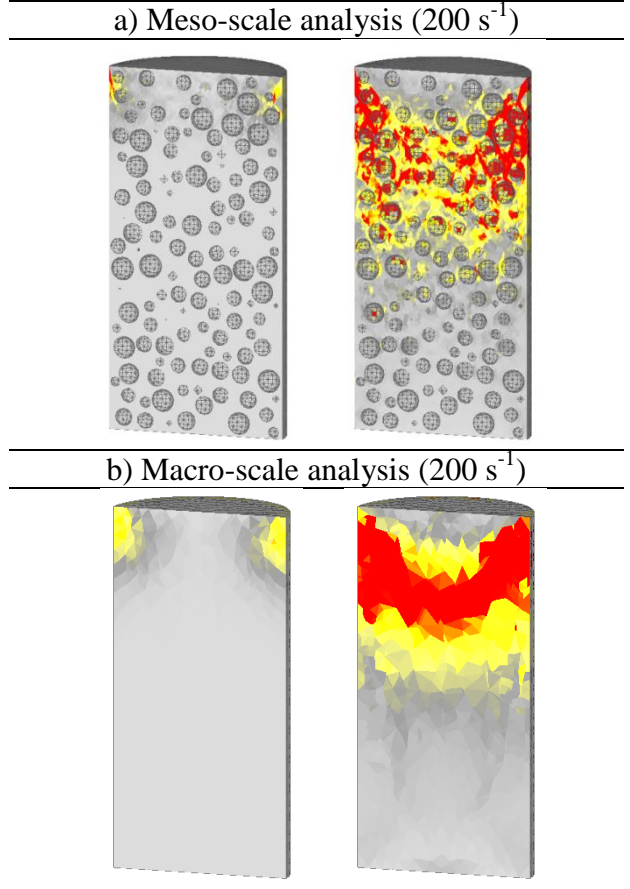


Figure 8: Evolution of damage under strain rate 200 s⁻¹: a) meso-scale analysis; b) macro-scale analysis

From the experiments it is evident that the contribution of strain rate effect to CDIF becomes significant for strain rate values greater than a critical value that is in the range 10¹ ÷ 10² s⁻¹. According to CEB recommendation [14], the dependence of CDIF on strain-rate is expressed as:

$$CDIF = \frac{f_{cd}}{f_{cs}} = \left[\frac{\dot{\epsilon}}{\dot{\epsilon}_s} \right]^{1.026\alpha_s} ; \text{ for } \dot{\epsilon} \leq 30 \text{ s}^{-1} \quad (2a)$$

$$CDIF = \gamma_s \left[\frac{\dot{\epsilon}}{\dot{\epsilon}_s} \right]^{\frac{1}{3}} ; \text{ for } \dot{\epsilon} > 30 \text{ s}^{-1} \quad (2b)$$

where f_{cs} and f_{cd} are the unconfined uniaxial compressive strengths from the static and dynamic tests, $\gamma_s = 10^{(6.156\alpha_s - 2.0)}$, $\alpha_s =$

$$1/(5 + 9 f_{cs}/f_{c0}), \quad \dot{\epsilon}_s = 30 \times 10^{-6} \quad \text{and} \\ f_{c0} = 10 \text{ MPa.}$$

The strain-rate effect on CDIF of concrete obtained by means of macro and meso-scale FE analysis and according to the CEB prediction formula (2) are shown in Fig. 9.

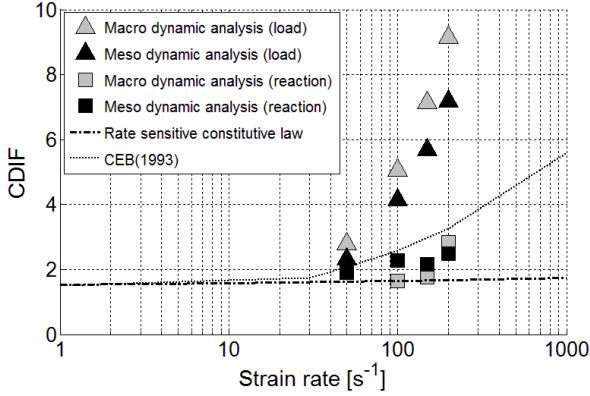


Figure 9: CDIF curves: numerical results, rate sensitive constitutive law and CEB formula

Both, the CDIF values measured at the top and at the bottom surfaces of the specimen (loading and reaction stresses) are shown and also compared with the used rate sensitive constitutive law. The first observation is that in both approaches the inertia activated in the damage zone of the specimen mainly controls the progressive increase of the peak loading stresses (apparent strength). Note that this progressive contribution of inertia automatically comes from the dynamic finite element analysis and not from the rate sensitive constitutive law (see Fig. 9). However, inertia has no significant influence on the peak reaction stresses. The peak reaction stress exhibits a trend that is close to that of the strain rate sensitive constitutive law, with almost no influence of structural inertia effects.

4 INFLUENCE OF INTERFACE ZONE (IZ)

The influence of the Interface Zone (IZ) on the compressive behavior of concrete is investigated in order to clarify whether the weaker properties of IZ can significantly contribute to the concrete response under both

static and dynamic compressive loading. The experimental measurement of the mechanical properties of IZ is rather difficult, however it is generally accepted that they are in the range of 30-80% of those of cement mortar. Another important factor is its thickness. In several numerical studies [16,19,27] the thickness is set to 0.2-0.8 mm to avoid numerical problems related to fine meshes along the IZ. In the present contribution the IZ thickness is set to 0.4 mm. The used material properties are summarized in Table 1. As mentioned above, the strength and fracture energy of the IZ are chosen to be approximately 50% of that of mortar, while the initial elastic modulus is the same for both materials. It is worth mentioning that the parameters of aggregate and cement mortar remain unchanged in both meso-scale models (with and without IZ).

The results obtained from the static analysis, in terms of stress-strain curves and failure mode, are shown in Figs. 10 and 11, respectively. From Fig. 11 can be seen that the explicit modeling of the IZ has negligible effect on the concrete compressive strength, while it has some influence in the pre and post-peak response. The low sensitivity of concrete compressive strength to the IZ strength is also reported in [28], where the effect of IZ on the failure of concrete is investigated through 2D meso-scale modeling approach. According to the authors, when the IZ strength is greater than or equal to 70% of that of mortar, concrete can be regarded as a two-phase medium comprising aggregate and mortar and the IZ can no longer be considered as the weakest area. Furthermore, the variation of the IZ strength has more impact on the direct tensile strength than on the compressive strength.

The evolution of damage for three loading stages (average axial strain) of mortar matrix is shown in Fig. 11. In the three-phase model (Fig. 11a) damage first localizes along the interface elements and only at higher stress levels the cracks propagate through the mortar matrix. Since the interface layers are damaged from relatively early loading stage (approximately 40% of the strength) the

material response is weaker in the pre-peak region (see Fig. 10).

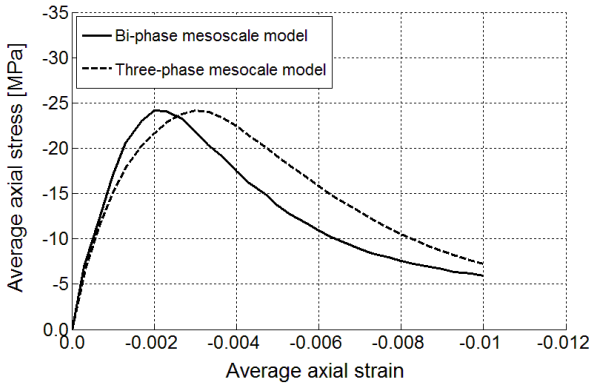


Figure 10: Uniaxial compressive test: average axial stress-strain curve

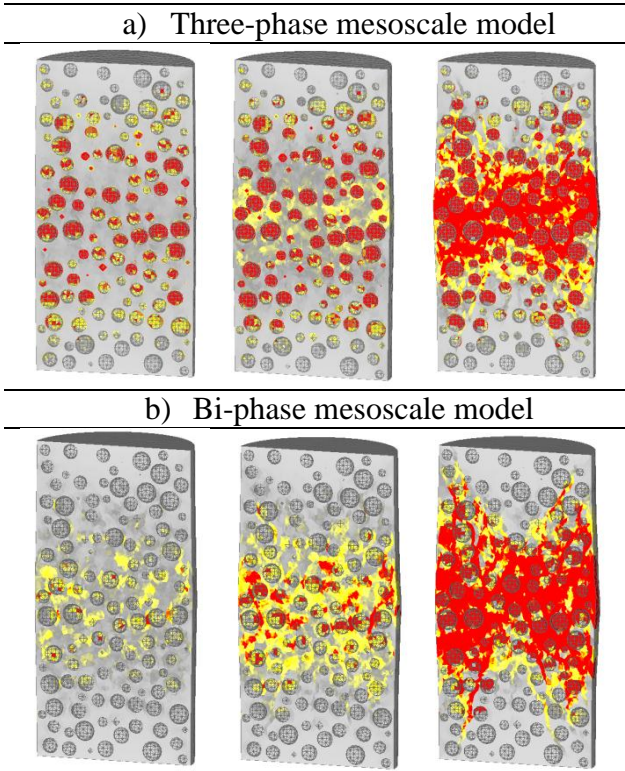


Figure 11: Evolution of damage in the static FE analysis: a) Three-phase meso-scale model and b) Bi-phase meso-scale model

In the bi-phase model (Fig. 11b) the cracks can only propagate in the mortar matrix; however higher strain values are observed in the thin mortar layers surrounding the aggregates. The final failure mode (Figs. 11a,b) is similar in both models. The influence of IZ on dynamic compressive

resistance is shown in Figs. 12,13. Figure 12 shows the stress-strain curves obtained with both models for the strain rate of 200 s^{-1} . It can be seen (Fig. 12) that the IZ has no influence on the dynamic compressive behavior of concrete, in terms of both, resistance and stress-strain response. The same has been observed for all analyzed strain rates and the results in terms of CDIF-curves are shown in Fig. 13. It can be noted that CDIF values obtained with both meso-scale models perfectly match. As confirmed by a recent study [10], the weaker link between aggregate pieces and mortar (IZ) does not contribute to CDIF.

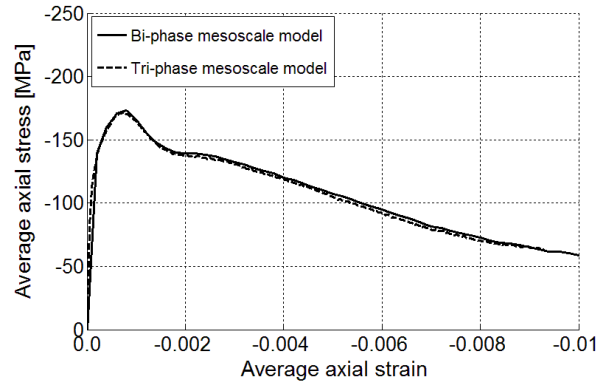


Figure 12: Dynamic meso-scale analysis, influence of IZ: average axial stress-axial strain curve (strain rate 200 s^{-1})

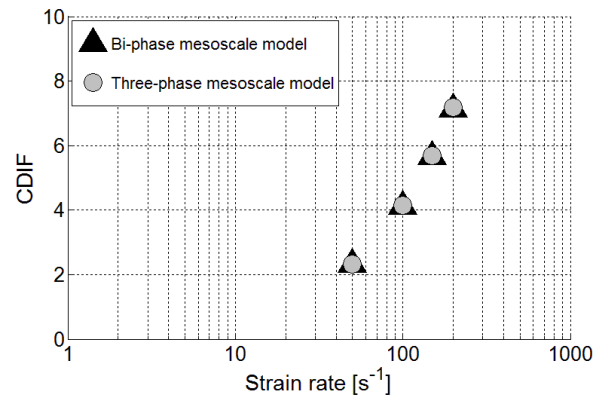


Figure 13: Dynamic meso-scale analysis, influence of IZ: CDIF-curves

5 CONCLUSIONS

In the present paper fracture of normal strength concrete cylinder under static and dynamic loading is studied numerically. 3D

finite element analysis was performed at meso and macro scale. Based on the results of the simulations the following can be concluded: (i) It is shown that for higher strain rates there is a progressive increase of resistance. However, this is the case only for the loading part of the cylinder. In contrary to this, the resistance on the reaction side of the specimen approximately follows the rate sensitive constitutive law. The main reason for progressive increase of resistance is damage-induced inertia which is automatically accounted for in dynamic finite element analysis; (ii) It is demonstrated that macro-scale approach is able to correctly predict dynamic compressive fracture of concrete. The failure mode in meso- and macro-scale approach is principally the same, however, the resistance of the macro model is slightly higher. The reason is due to the fact that in the meso-scale analysis the aggregates exhibit no damage and no rate sensitivity (linear elastic); (iii) The interface zone (IZ) has relatively small influence on the compressive response of concrete. This was observed for static and dynamic loading conditions.

REFERENCES

- [1] Ožbolt J., Bošniak J. and Sola E., 2013. Dynamic fracture of concrete compact tension specimen: experimental and numerical study. *Int. J. Solids Struct.* **50**:4270-4278.
- [2] Ožbolt J., Sharma A., Irhan B. And Sola E., 2014. Tensile behavior of concrete under high loading rates. *Int. J. Impact Engng.* **69**:55-68.
- [3] Pająk M., 2001. The influence of the strain rate on the strength of concrete taking into account the experimental techniques. *Architecture civil engineering environment.* **3**:77-86.
- [4] Abrams D.A., 1917. Effect of rate of application of load on the compressive strength of concrete. *ASTM J.* **17**:364-377.
- [5] Evans R.H., 1942. *Effect of rate of loading on the mechanical properties of some materials.* J. Inst. Civil. Engrs.
- [6] Hughes B.P. and Watson A.J., 1978. Compressive strength and ultimate strain of concrete under impact loading. *Ibid.* **30**(105):189-199.
- [7] Malvern L.E. and Ross C.A., 1985. Dynamic response of concrete and concrete structures. Second Annual Technical Report. AFOSR contr. No. F49620-83-K007.
- [8] Ross C.A., Thompson P.Y. and Tedesco J.W., 1989. Split-Hopkinson pressure-bar tests on concrete and mortar in tension and compression. *ACI Mater. J.* **86**:475-481.
- [9] Tedesco J.W. and Ross C.A., 1998. Strain-dependent constitutive equations for concrete. *ASME.* **120**:398-405.
- [10] Grote D.L., Park S.W. and Zhou M., 2001. Dynamic behavior of concrete at high strain-rates and pressures: I. Experimental characterization. *Int. J. Impact Engng.* **25**:869-886.
- [11] Hao Y., Hao H., Jiang G.P. and Zhou Y., 2013. Experimental confirmation of some factors influencing dynamic concrete compressive strengths in high-speed impact tests. *Cement and Concrete Research.* **52**:63-70.
- [12] Salloum Y.A., Almusallam T., Ibrahim S.M., Abbas H. and Alsayed S., 2015. Rate dependent behavior and modeling of concrete based on SHPB. *Cement & Concrete Composites.* **55**:34-44.
- [13] Chen X.W., Lv T. and Chen G., 2018. Experimental and Numerical Studies on the Dynamic Behaviors of Concrete Materials Based on the Waveform Features in SHPB Tests. *EPJ Web of Conferences (DYMAT) 2018.*

- [14]Comite Euro-International du Beton 1993. CEB-FIP model code 1990. Redwood Books, Trowbridge, Wiltshire, UK.
- [15]Li Q.M. and Meng H., 2003. About the dynamic strength enhancement of concrete-like materials in a split Hopkinson pressure bar test. *Int. J. Solids Struct.* **40**:343-360.
- [16]Hao Y., Hao H. and Li Z.X., 2013. Influence of end friction confinement on impact tests of concrete material at high strain rate. *In. J. Impact. Engng.* **60**:82-106.
- [17]Bishoff P.H. and Perry S.H., 1991. Compressive behavior of concrete at high strain rates. *Materials and Structures.* **24**:425-450.
- [18]Sharma A. And Ožbolt J., 2014. Influence of high loading rates on behavior of reinforced concrete beams with different aspect ratios–A numerical study. *Engineering Structures.* **79**:297-308.
- [19]Huang Y., Zhenjun Y. and Guohua L., 2016. X-ray computed tomography image-based meso-scale dynamic fracture of concrete under compression: monte carlo simulations. *Proc. of the 9th Inter. Conf. on Fract. Mech. of Conc. & Conc. Struct (FraMCoS-9)*,
- [20]Ožbolt J., 1998. MASA – Macroscopic Space Analysis. Internal Report, Institute für Werkstoffe im Bauwesen, Universität Stuttgart, Germany.
- [21]Ožbolt J., Sharma A. and Reinhardt H.W., 2011. Dynamic fracture of concrete - compact tension specimen. *Int. Jr. Solids Struct.* **48**:1534-1543.
- [22]Mondal P., Shah S.P. and Marks L.D., 2009. Nanomechanical properties of interfacial transition zone in concrete. *Proc. of Nanotechnology in Construction 3*, Springer:315–320.
- [23]Ožbolt J., Li Y. and Kožar I., 2001. Microplane model for concrete with relaxed kinematic constraint. *Int. J. Solids Struct.* **38**:2683-2711.
- [24]Bažant Z.P., Adley M.D., Carol I., Jirasek M., Akers S.A., Rohani B. et al. 2000a. Large-strain generalization of microplane model for concrete and application. *J. Engg. Mech. (ASCE).* **126**(9):971-980.
- [25]Bažant Z.P., Caner F.C., Adley M.D. and Akers S.A. 2000b. Fracturing rate effect anmd creep in microplane model for dynamics. *J. Engg. Mech. (ASCE).* **126**(9):962-970.
- [26]Bažant Z.P. and Oh B.H., 1983. Crack band theory for fracture of concrete. *Materials and Structures, RILEM.* **16**(93):155-177.
- [27]Song Z and Lu Y., 2012. Mesoscopic analysis of concrete under excessively high strain rate compression and implications on interpretation of test data. *Int. J. Impact Engng.* **46**:41-55.
- [28]Zhang S., Zhang C., Liao L. and Wang C., 2018. Numerical study of the effect of ITZ on the failure behavior of concrete by using particle element modelling. *Construction and Building Materials* **170**:776-789.